OPEN ACCESS

Original research

Spatial dissection of tumour microenvironments in gastric cancers reveals the immunosuppressive crosstalk between *CCL2*+ fibroblasts and *STAT3*-activated macrophages

Sung Hak Lee,[1] Dagyeong Lee ,[2] Junyong Choi,[2,3] Hye Jeong Oh,[2] In-Hye Ham,[2,4] Daeun Ryu,[5] Seo-Yeong Lee,[5,6] Dong-Jin Han,[5,6] Sunmin Kim,[5,6] Youngbeen Moon,[5,6] In-Hye Song,[7] Kyo Young Song,[8] Hyeseong Lee,[1] Seungho Lee,[9] Hoon Hur,[2,3,4] Tae-Min Kim[5,10,11]

► Additional supplemental material is published online only. To view, please visit the journal online (https://doi.org/10.1136/gutjnl-2024-332901).

For numbered affiliations see end of article.

Correspondence to
Dr Tae-Min Kim; tmkim@catholic.ac.kr and Dr Hoon Hur; hhcmc75@ajou.ac.kr

SHL and DL are joint first authors.

Received 23 May 2024
Accepted 4 November 2024

To cite: Lee SH, Lee D, Choi J, *et al*. *Gut* Epub ahead of print: [*please include* Day Month Year]. doi:10.1136/gutjnl-2024-332901

ABSTRACT

Background A spatially resolved, niche-level analysis of tumour microenvironments (TME) can provide insights into cellular interactions and their functional impacts in gastric cancers (GC).

Objective Our goal was to translate the spatial organisation of GC ecosystems into a functional landscape of cellular interactions involving malignant, stromal and immune cells.

Design We performed spatial transcriptomics on nine primary GC samples using the Visium platform to delineate the transcriptional landscape and dynamics of malignant, stromal and immune cells within the GC tissue architecture, highlighting cellular crosstalks and their functional consequences in the TME.

Results GC spatial transcriptomes with substantial cellular heterogeneity were delineated into six regional compartments. Specifically, the fibroblast-enriched TME upregulates epithelial-to-mesenchymal transformation and immunosuppressive response in malignant and TME cells, respectively. Cell type-specific transcriptional dynamics revealed that malignant and endothelial cells promote the cellular proliferations of TME cells, whereas the fibroblasts and immune cells are associated with procancer and anticancer immunity, respectively. Ligand-receptor analysis revealed that *CCL2*-expressing fibroblasts promote the tumour progression via JAK-STAT3 signalling and inflammatory response in tumour-infiltrated macrophages. *CCL2*+ fibroblasts and *STAT3*-activated macrophages are co-localised and their co-abundance was associated with unfavourable prognosis. We experimentally validated that *CCL2*+ fibroblasts recruit myeloid cells and stimulate *STAT3* activation in recruited macrophages. The development of immunosuppressive TME by *CCL2*+ fibroblasts were also validated in syngeneic mouse models.

Conclusion GC spatial transcriptomes revealed functional cellular crosstalk involving multiple cell types among which the interaction between *CCL2*+ fibroblasts and *STAT3*-activated macrophages plays roles in establishing immune-suppressive GC TME with potential clinical relevance.

WHAT IS ALREADY KNOWN ON THIS TOPIC

⇒ Tumour microenvironments (TME) exhibit notable cellular heterogeneity, a characteristic feature of various cancers, including gastric cancers (GC).
⇒ Interactions and functional interplay among diverse cell types within the GC TME are implicated in cancer progression.
⇒ Previous studies have identified key cellular components within the GC TME; however, there is a lack of comprehensive insights derived from spatially relevant methods that delineate their interplay.

INTRODUCTION

Gastric cancers (GC) are a major global concern because they cause high cancer-related morbidity and mortality.[1] Although the mutational configuration revealed by large-scale sequencing efforts can guide the selection of molecular targets, the effect is only modest,[2] with *HER2* positivity and trastuzumab to target it as the only currently approved therapeutic regimen.[3] The standard therapeutic modalities for GCs—early intervention, surgical resection and cytotoxic agent-based chemotherapy such as 5-fluorouracil—have not improved much in decades.[4]

The disease heterogeneity responsible for disease initiation, maintenance and progression is largely attributed to transcriptional and cellular heterogeneity. Recently developed single-cell RNA sequencing (scRNA-seq) technologies directly evaluate the transcriptional heterogeneity of tissues with single cell resolution, which facilitates the delineation of subtypes among the major cell types in tumour microenvironments (TMEs). Currently available scRNA-seq GC datasets[5–8] could also serve as valuable resources for elucidating the cellular heterogeneity of GC and facilitating the identification of cellular subpopulations associated with particular phenotypes of interest, such as drug resistance, metastatic risk and cellular plasticity.

WHAT THIS STUDY ADDS

⇒ Using Visium-based spatial transcriptomics, we identified six spatial clusters, or niches that exhibit regionally concordant enrichment of major cell types within the GC TME.

⇒ Cellular crosstalks in GC TME were delineated into major cell types acting as regulators and targets along with their functional consequences, highlighting key players of the inflammatory response with stromal infiltrations, *CCL2*+ fibroblasts and *STAT3*-activated macrophages.

⇒ We propose a cellular composition-based classification system, categorising GCs into epithelial, immunogenic and fibrotic subtypes with validation by tissue microarrays.

HOW THIS STUDY MIGHT AFFECT RESEARCH, PRACTICE OR POLICY

⇒ The comprehensive map of cellular crosstalk within the GC TME serves as a valuable resource for identifying targetable cell subtypes and their associated markers, advancing GC diagnostics and therapeutic development.

⇒ *CCL2*+ fibroblasts and their activation of the JAK-STAT signalling pathway in macrophages represent significant cellular responses in GC, characterised by stromal cell infiltration and offering potential targets to enhance anticancer immunity in GC therapeutics.

⇒ The cellular classification system offers histology-relevant GC subtype classifications that can benefit GC diagnostics and treatment strategies.

In a previous study,[9] we performed tumour depth-aware scRNA-seq to leverage spatial information by separately analysing layer-specific scRNA-seq data from diffuse-type GCs (ie, normal tissues and superficial vs deep tumour layers). By assuming that the transition from superficial to deep layers reflected tumour progression, we were able to identify cellular subpopulations that exhibited differential expression along that transition. Recently, high-resolution mapping of the spatial organisation of cells has become possible, and it generates thousands of transcriptome profiles per sample, each conserved in its anatomical, tissue architecture context.[10] In addition to spatially unravelling cellular heterogeneity, these technologies could be used to interrogate the spatial relationships among malignant cells and TME cells and to explore the functional consequences of those relationships as spatial patterns of oncogenic crosstalk.

In this study, we used Visium spatial transcriptome technology[11] to analyse nine GC specimens (GC1–GC9). We first established three GC subtypes based on cell abundance to ensure that the histology of each GC robustly represented the cellular composition of each given GC tissue. We established a landscape of functional cellular crosstalk to represent the functional consequences of cellular interactions between regulator and target cells. Among those interactions, we highlight that *CCL2*+ fibroblasts regulate the JAK-STAT signalling of macrophages as a key immunomodulatory effect of fibroblast infiltration in a GC TME. The cellular interactions and their molecular consequences were validated using *in vitro* and *in vivo* experimental models, and we further explored their relevance to clinical outcomes.

METHODS

Detailed methods are described in online supplemental methods.

Patient and public involvement

Patients and/or the public were not involved in the design, or conduct, or reporting, or dissemination plans of this research.

RESULTS

Spatial cellular maps of three GC subtypes

Nine surgically removed primary GCs were obtained from nine patients and subjected to spatial transcriptomics using Visium technologies (10X Genomics). The clinicopathological features of the nine patients with GC are available in online supplemental table S1. Overall, the spatial transcriptomics data yielded 1882–4274 spots per histological section in each of the nine cases (median, 3491 spots) (online supplemental table S2). Spot-level cell deconvolution was performed with respect to 11 cell types, as explained in our previous report of scRNA-seq data from five GC cases.[9] Epithelial cells were further divided into tumour and normal cells (malignant and normal epithelium, respectively), so the deconvoluted cellular abundance per spot was examined for 12 cell types (details available on online supplemental methods and online supplemental figure S18). The summary of the deconvoluted cellular abundances, categorised on a case-by-case basis, is shown in figure 1A. Notably, although the cellular compositions reveal substantial heterogeneity, the clustering of the deconvoluted cellular abundance data distinguishes three GC subtypes: immunogenic, epithelial and fibrotic. These subtypes are to some extent consistent with the Lauren classification, for example, intestinal-type GCs were classified as either the immunogenic or epithelial GC subtype, and all the fibrotic GCs were classified as the diffuse-type. The main cellular components of the three epithelial GCs (GC3, GC5 and GC7) were malignant or normal epithelial cells. The three immunogenic GCs were either microsatellite unstable (microsatellite instability (MSI)-positive; GC1) or Epstein-Barr virus (EBV)-positive GCs (GC2 and GC8) in microsatellite stable (MSS) GCs, consistent with their high level of tumour-infiltrating immune cells, as previously reported.[12] CD4+ and CD8+ T cells are major immune cell components in these GC types. Among the five diffuse types of GCs, three (GC4, GC6 and GC9) were annotated as fibrotic GCs with high levels of tumour-infiltrating fibroblasts.

Spatial cellular maps for selected examples of the three GC categories (GC1/GC3/GC4 representing immunogenic, epithelial and fibrotic GCs, respectively) are depicted in figure 1B. Two types of spatial maps are represented as those based on regional annotations by pathologists (left panels) and deconvoluted spot-level cellular abundances, which highlight cell types with a predominant presence or the highest abundances per individual spot, respectively (middle panels). To align with the regional annotation by pathologist, cell types of individual spots were summarised into 'malignant spot', 'normal epithelial spot', 'stromal spot' (combining fibroblasts and endothelium) and 'immune spot' (comprising eight immune cell types). The spatial maps of the remaining cases are shown in online supplemental figure S1, with details on the histological images and the expression of cell type-specific markers available in online supplemental figure S2. And, we also analysed the abundance of 12 individual cell types for each GC subtypes (online supplemental note 1). As shown by those results, the cellular abundance in GC microenvironments can be classified into at least three GC subtypes, and spot-level correlations across cell types imply that they are regionally associated in GC TMEs. Thus, our spatially resolved cellular abundance data offer insights into the major cell types of GC and their spatial relationships within GC TME architectures.

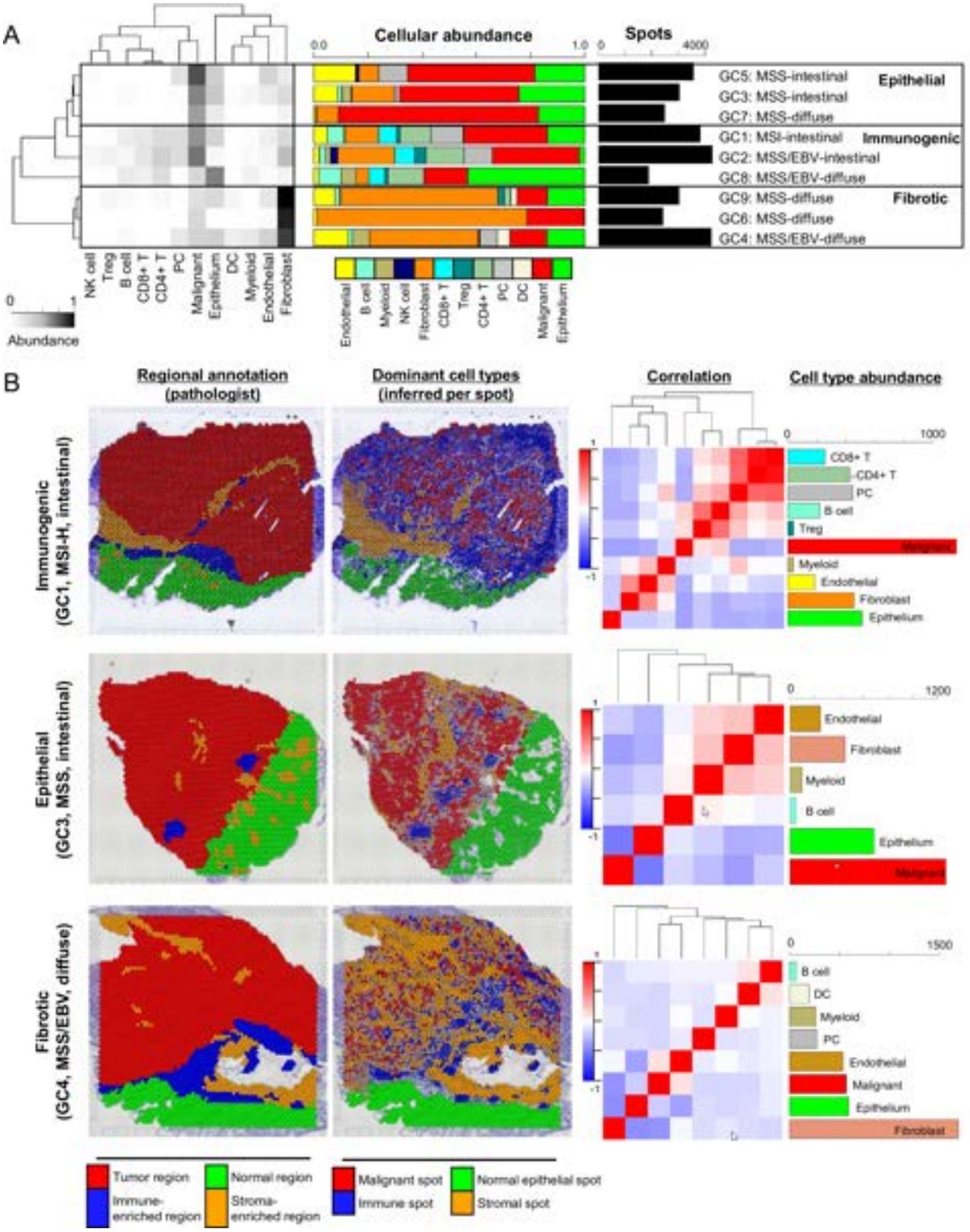

Figure 1 Classification of three gastric cancer (GC) subtypes. (A) A heatmap (left) and bar plots (middle) illustrate the cellular abundances of 12 cell types in nine GC cases (GC1–GC9). Hierarchical clustering categorised the nine GCs into three GC subtypes: epithelial, immunogenic and fibrotic, which are characterised by the dominance of malignant cells, immune cells and fibroblasts, respectively. Additional bar plots show the number of spots present in each case (right). (B) For the cases chosen to represent each subtype—immunogenic (GC1), epithelial (GC3) and fibrotic (GC4) GCs—histological annotations of spots determined by pathologists (left) are shown alongside the dominant cell types of individual spots determined by deconvolution (ie, cell types with the highest enrichment; middle). A correlative heatmap also demonstrates the relationships between cell types based on spot-level correlations of cellular abundances (right). DC, dendritic cell; EBV, Epstein-Barr virus; MSI-H, microsatellite instability-high; MSS, microsatellite stable; NK, natural killer; PC, plasma cell; Treg, regulatory T cell.

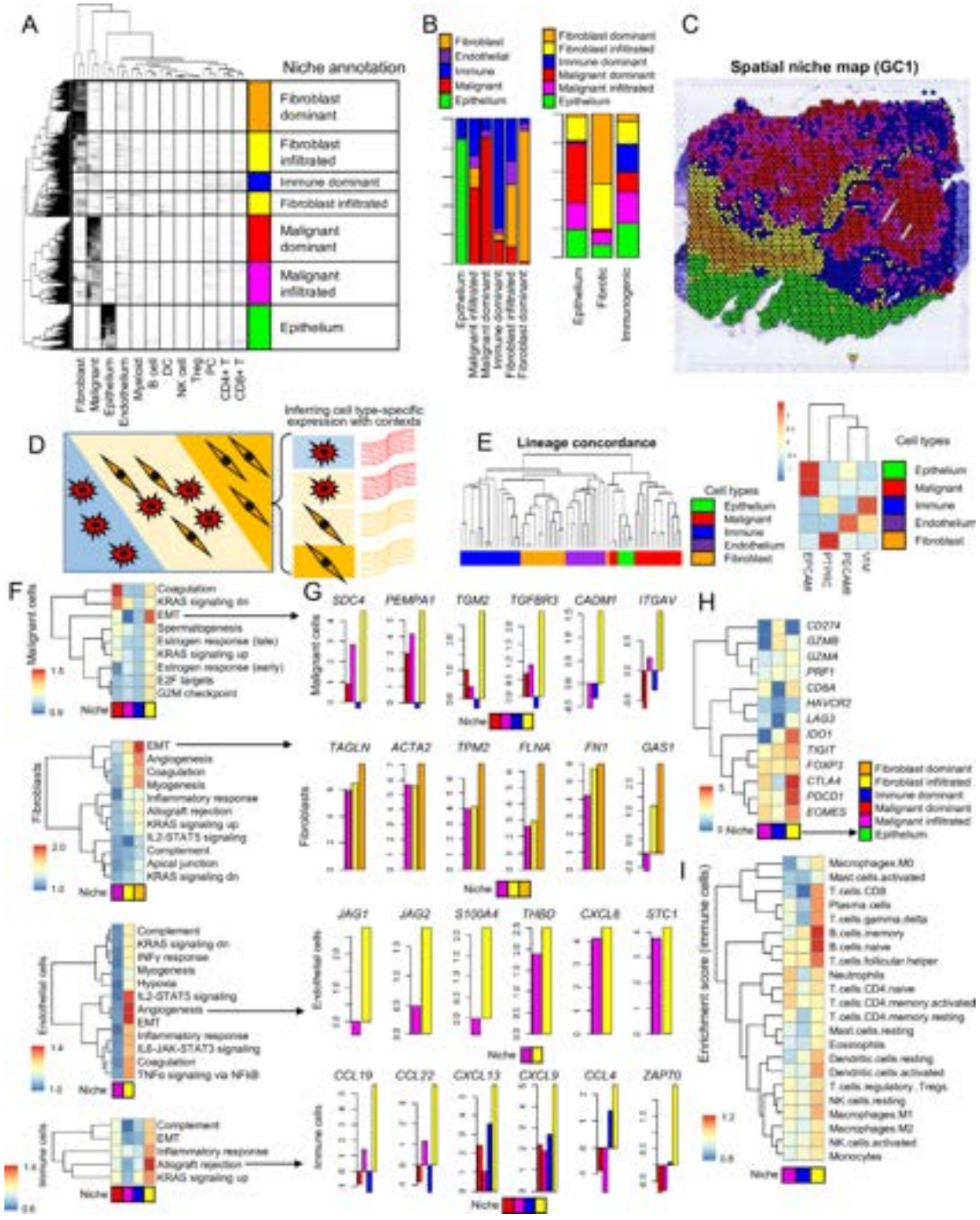

Figure 2 Spatial niche in gastric cancer (GC) tumour microenvironments (TME) and their associated transcriptional dynamics. (A) The cellular compositions of all GC spots obtained across nine cases (n=29 808) were subjected to hierarchical clustering, which segregated them into six niche categories. The six niches are annotated with respect to the level of TME infiltration and predominant cell types. (B) The distribution and proportion of cellular subtypes within each niche and their prevalence in the three GC subtypes. (C) The spatial representation of niches in GC1. (D) A schematic shows that malignant cells and fibroblasts are either isolated (left and right) or intermingled (middle) in three different niches (left, middle and right). Cell type-specific expression profiles can be inferred and compared with respect to niches, for example, malignant cell expressions inferred from the left and middle niches provide information about the transcriptional dynamics of malignant cells with fibroblast infiltration. (E) A high degree of lineage concordance was observed for the cell type-specific expression inferred across niches. The expression of four cell type-specific markers was also concordant for deconvoluted cell type-specific expression as shown in a heatmap. (F) Functional enrichment analyses for four cell types (malignant cells, fibroblasts, endothelial and immune cells) are shown in individual heatmaps as evaluated across different niches (Hallmark gene set, false discovery rate (FDR) <0.1). (G) Selected functions are indicated by arrows (eg, epithelial-to-mesenchymal transition (EMT) in malignant cells), and their relevant genes are shown to indicate their expression changes across niches. The niche colour schemes match those in panel (A). (H) and (I) show the expression of selected immune-related genes in immune cells and the CIBERSORT-estimated abundance of 22 immune cell types across niches, respectively. DC, dendritic cell; IFN, interferon; IL, interleukin; NFκB, nuclear factor-kappa B; NK, natural killer; PC, plasma cell; TNF, tumour necrosis factor; Treg, regulatory T cell.

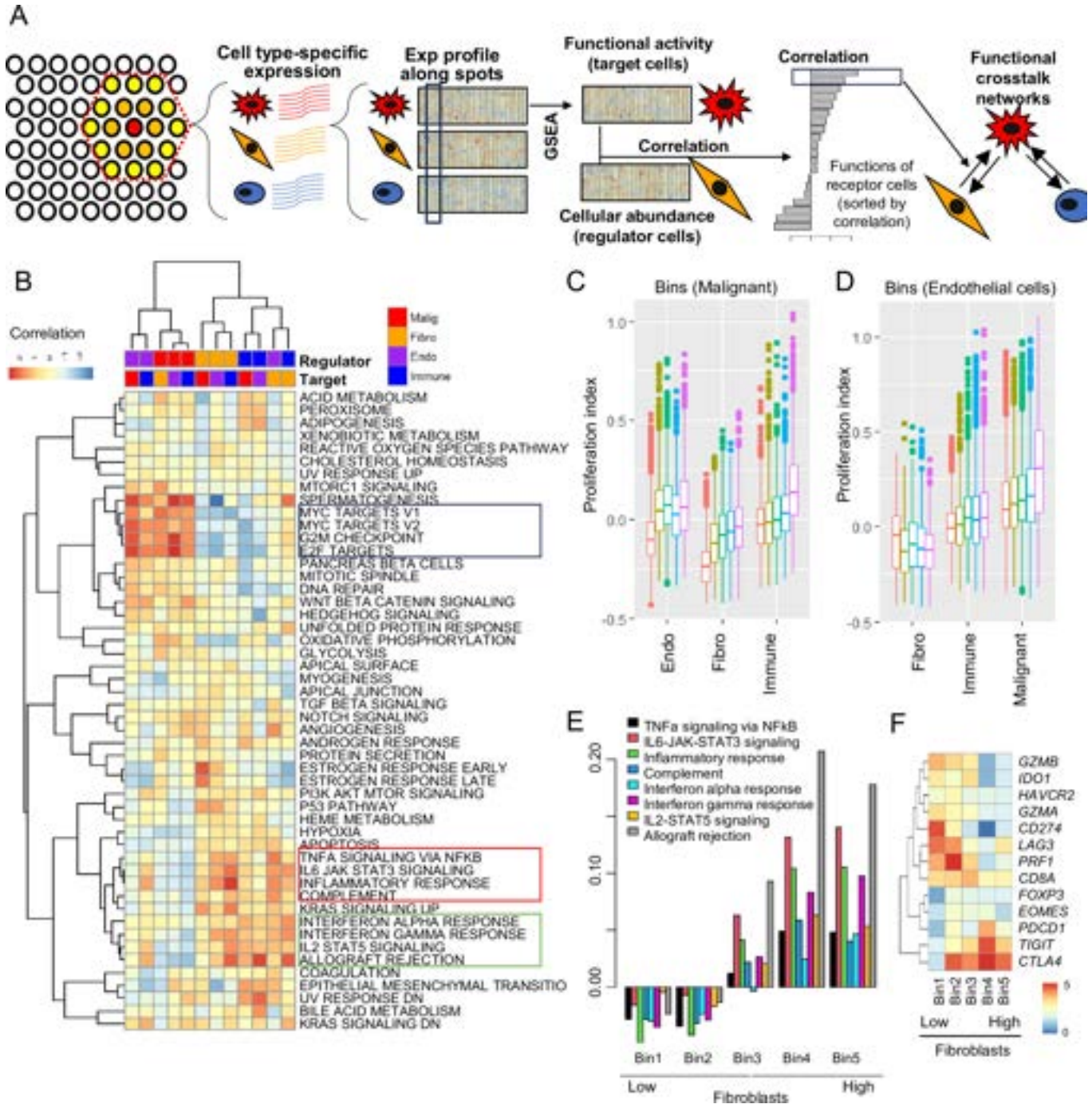

Figure 3 Landscape of cellular crosstalk and its functional consequences in gastric cancer (GC) tumour microenvironments (TME). (A) The schematic illustrates the process of inferring cell type-specific expression at the individual spot level for the functional crosstalk analysis. Each spot, along with its neighbouring 18 spots (six nearest N1 and 12 next-nearest N2 spots, in orange and yellow, respectively), is analysed to deconvolute the cell type-specific expression of the five major cell types. The inferred cell type-specific expression was then subjected to a gene set enrichment analysis (GSEA) to develop the cell type-specific functional score profiles. Correlations between the functional scores of target cells and the abundance of regulator cells across spots indicate functional relationships between target and receptor cells. (B) Functional interactions among the four cell types of interest (malignant cells, endothelial cells, immune cells and fibroblasts) were analysed pairwise, resulting in 16 different functional consequences that are depicted in the heatmap as a landscape of cellular crosstalk in GC TMEs. This heatmap shows the correlation levels for various functional terms, with each column corresponding to a specific regulator and target cell pairing, as indicated in the top panels. For instance, the first column shows how endothelial cells as regulators might affect malignant cells as targets, possibly leading to increased MYC target expression in the latter. Three boxes highlight functional sets associated with the infiltration of malignant and endothelial cells (black), immune cells (green) and fibroblasts (red). (C) Spots were categorised into five bins based on the level of malignant cell infiltration, and the proliferation index was calculated using genes related to cellular proliferation across bins. An overall increase in the proliferation indexes of cells in the GC TME was observed to correlate with increasing levels of malignant cell infiltration. (D) The proliferation index was similarly calculated across bins representing the level of endothelial cell infiltration. (E) Across bins representing the level of fibroblast infiltration, the activity levels of eight immune-related functions are shown. (F) Similarly, the expression levels of immune-related genes are shown across the fibroblast bins. IL, interleukin; TNF, tumour necrosis factor.

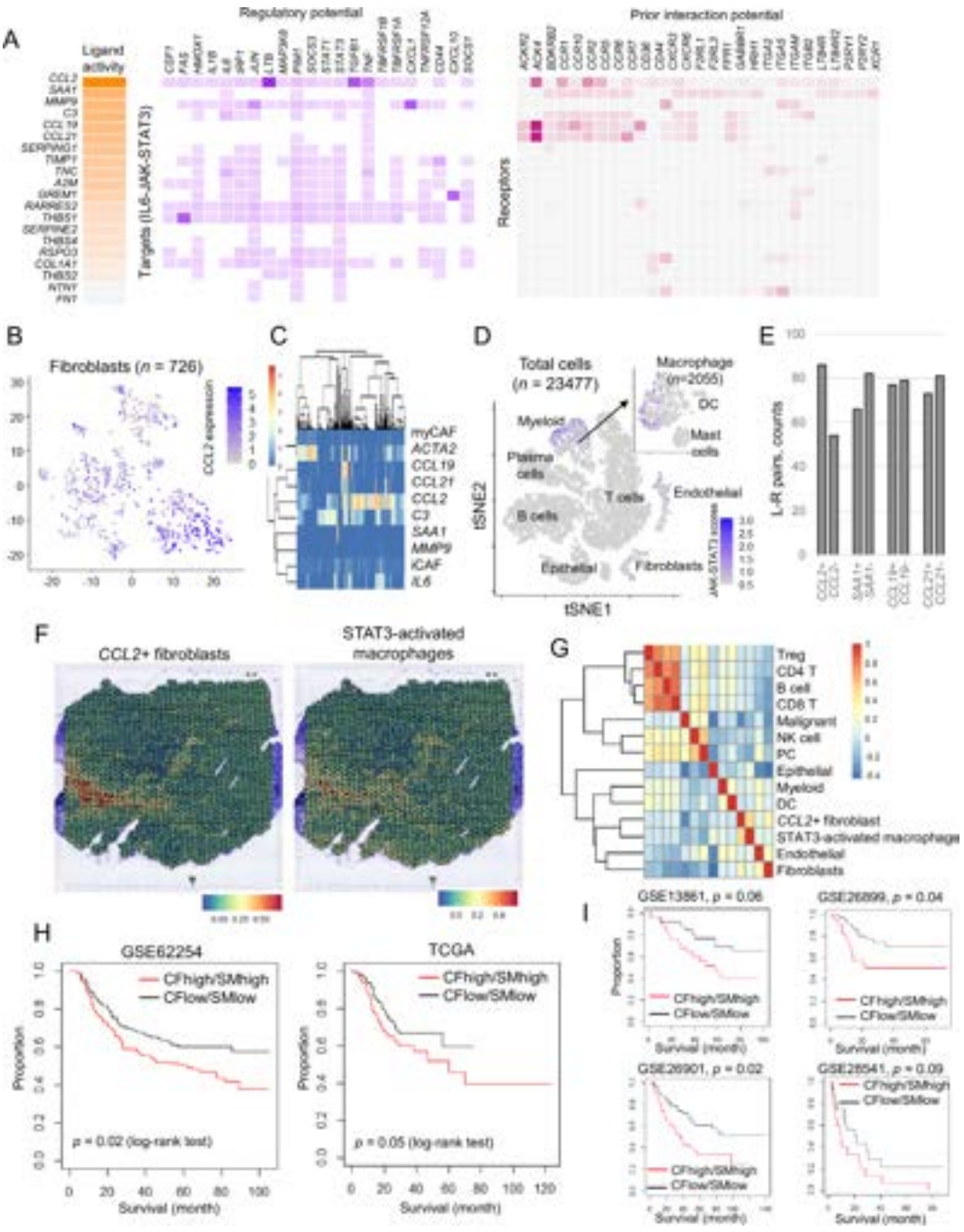

Figure 4 *CCL2*+ fibroblasts and *STAT3*-activated macrophages with spatial co-localisation and clinical outcomes. (A) A NicheNet analysis reveals the top ligands associated with cellular interactions between fibroblasts and immune cells as regulators and target cells, respectively. This analysis highlights *CCL2* as having the top ligand activity in fibroblasts. The interacting target genes and receptor genes are also demonstrated. (B) A t-Distributed Stochastic Neighbour Embedding (tSNE) plot shows the distribution of *CCL2* expression across 716 fibroblasts in the single-cell RNA sequencing (scRNA-seq) data. (C) A correlative heatmap shows the level of expression for ligands, including *CCL2* (selected in figure 4A), and inflammatory cancer-associated fibroblast (iCAF) and myofibroblastic cancer-associated fibroblast (myCAF) scores with their cognate markers of *IL6* and *ACTA2*, respectively. (D) All gastric cancer (GC) tumour microenvironment (TME) cells (n=23 477) in the scRNA-seq data are shown in a tSNE plot, which indicates that JAK-STAT3 signature scores are largely limited to myeloid cells. The inset shows that myeloid cells with JAK-STAT3 signature scores are further limited to macrophages. We define *STAT3*-activated macrophages as those with high JAK-STAT3 scores. (E) The number of significant ligand-receptor pairs in CellphoneDB analysis are shown in y-axis. *CCL2*+ represents those identified in *CCL2*+ fibroblasts and *STAT3*-activated macrophages. (F) In a GC1 spatial map, the spot-level scores representing the abundance of *CCL2*+ fibroblasts and *STAT3*-activated macrophages show a concordant pattern suggesting that the two cell types are co-localised. (G) A heatmap shows the correlation level across all spots for the cellular abundance of 12 cell types and the scores for *CCL2*+ fibroblasts and *STAT3*-activated macrophages. (H) In two public GC bulk-level transcriptome datasets (Asian Cancer Research Group (ACRG) and The Cancer Genome Atlas (TCGA)), patients whose samples were *CCL2*+ fibroblast high (CF-high) and *STAT3*-activated macrophage-high (SM-high) (shown in red) had substantially worse clinical outcomes than those whose samples were *CCL2*+ fibroblast low (CF-low) and *STAT3*-activated macrophage-low (SM-low) (shown in black). (I) Four additional GC cohorts showed similar results. DC, dendritic cell; NK, natural killer; PC, plasma cell; Treg, regulatory T cell.

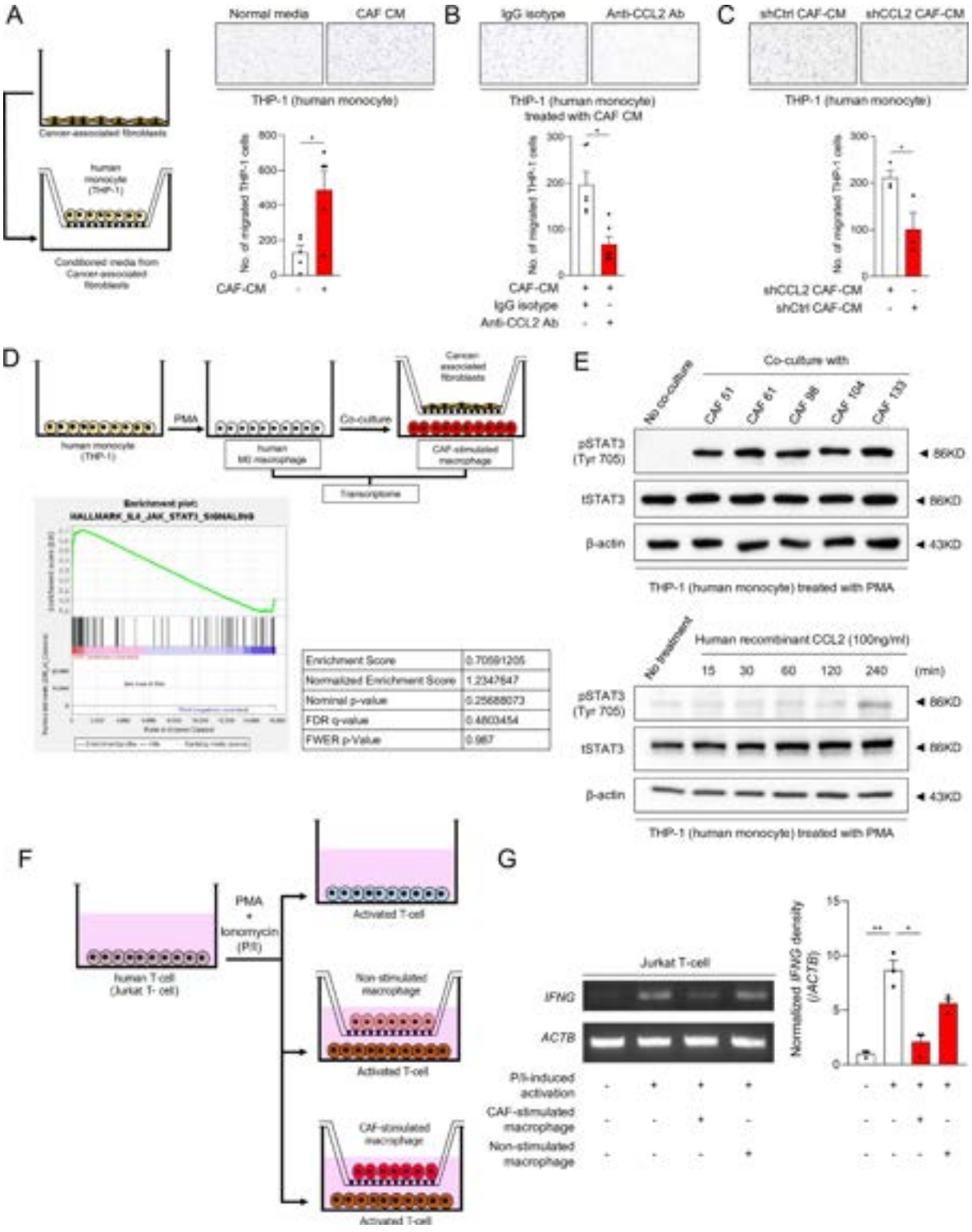

Figure 5 *CCL2*+ cancer-associated fibroblasts (CAFs) recruit myeloid cells and activate the phosphorylation of STAT3 in macrophages. (A) A transwell migration assay showed that CAF-conditioned medium (CM) increased the migration ability of human monocyte cell line (THP-1) cells. Paired t-test. *P<0.05. (B–C) A transwell migration assay showed that 200 ng/mL anti-CCL2 neutralising antibody (B) and *CCL2* knockdown CAF-CM (C) decreased the migration ability of THP-1 cells. Paired t-test. *P<0.05. (D) A gene set enrichment analysis showed that JAK-STAT3 signalling genes are upregulated in CAF-stimulated macrophages, compared with non-stimulated macrophages. (E) Various CAF cells activated STAT3 phosphorylation in phorbol 12-myristate 13-acetate (PMA)-induced macrophages (top). Treatment with recombinant CCL2 (100 ng/mL) activated STAT3 phosphorylation in PMA-induced macrophages in a time-dependent manner (bottom). (F) THP-1 cells were differentiated into macrophages for 48 hours and then co-cultured with CAFs. Jurkat cells were activated with PMA/ionomycin (P/I) treatment for 3 hours and then co-cultured with macrophages for 6 hours. (G) P/I-induced activation of Jurkat cells increased *IFNG* expression. However, co-culture with CAF-stimulated macrophages reduced *IFNG* expression in activated Jurkat cells. Kruskal-Wallis test, uncorrected Dunn's post hoc test. *P<0.05, **p<0.01. FDR, false discovery rate; FWER, family wise error rate.

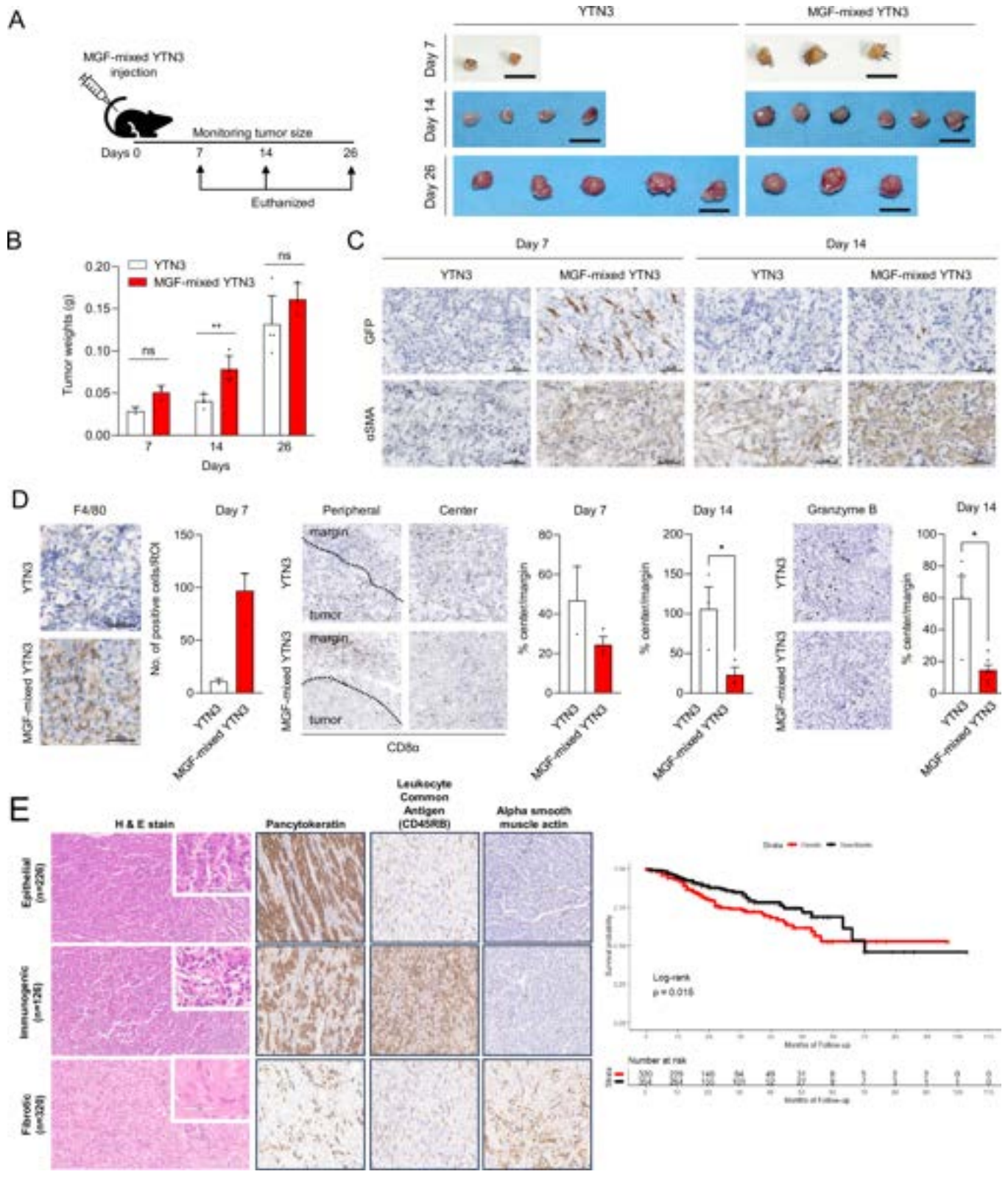

Figure 6 *CCL2*+ fibroblasts induce an immunosuppressive tumour microenvironments (TME) in vivo. (A) YTN3 cells with and without mouse gastric fibroblasts (MGFs) were subcutaneously injected into C57BL/6J mice. The established tumours were harvested on days 7, 14 and 26. (B) Weights of the harvested tumours. Mann-Whitney U test and t-test. **P<0.001. (C) Immunohistochemistry (IHC) for GFP (injected MGF) and α-smooth muscle actin (α-SMA) (total fibroblasts) in day 7 and day 14 tumours. Scale bar=50 µm. (D) IHC for F4/80 (macrophages), CD8α (CD8+ T cells) and granzyme B in mouse tumours. Positive cells per region of interest (ROI) were counted using QuPath (t-test, *p<0.05). Scale bar=50 µm. (E) Left panel: representative H&E (×200) and IHC (×400) images of the three gastric cancer (GC) subtypes. The epithelial group (n=226) showed a high density of GC cells in the H&E stain and high pan cytokeratin IHC expression. The immunogenic group (n=126), with enrichment of immune cells, was positive for CD45RB proteins. The fibrotic group (n=320) showed predominant fibrosis supported by high actin expression. Right panel: survival curves for each of the three GC subtypes in a patient cohort (Kaplan-Meier survival analysis with log-rank test, p=0.0023).

Spatially resolved cellular and transcriptional dynamics with respect to GC TME architecture

To regionally dissect the spatial cellular heterogeneity within each GC TME, we regionally categorised the spots while taking into account the varying cellular constituents and their regional adjacency (online supplemental note 2 and online supplemental figure S13). The hierarchical clustering of all the spots in the nine GCs (n=29 808) with respect to the cellular abundance in each spot and its neighboring spots revealed six regional categories, each with varying cellular components and extents of TME infiltration (figure 2A). The resulting categories, which we call 'niches', were annotated based on their cellular composition and dominant cell types. For instance, those primarily consisting of normal and malignant epithelial cells are designated as epithelial-dominant and malignant-dominant niches, respectively. Those with a prevalence of fibroblasts are called fibroblast-dominant niches. The remaining categories, which are marked by the infiltration of diverse cell types, are called malignant-infiltrated, fibroblast-infiltrated and immune-dominant niches. Figure 2B delineates the cellular compositions within the six identified niches and correlates those niches with the three distinct GC subtypes. The cellular compositions of 12 cell types across six niche types are also available in online supplemental figure S3. A detailed spatial niche map for a representative immunogenic GC case (GC1) is presented in figure 2C. This map elucidates the distribution of tissue architecture in the GC, highlighting the spatial confinement of malignant-dominant niches (red) and fibroblast-dominant niches (orange). The malignant-infiltrated niches (magenta) and fibroblast-infiltrated niches (yellow) appear to be intermediate zones and are encircled by regions characterised by a high density of immune cells (immune-dominant niches, blue). Epithelial-dominant niches (normal epithelium, green) appear as isolated regions within the tissue. Spatial maps for the other GC cases are provided in online supplemental figure S4 and online supplemental note 3. Therefore, the spatial architecture of GC is largely governed by cellular dominance between malignant cells and fibroblasts, along with the delineating presence of immune cells in immunogenic and epithelial GCs. The depletion of immune cells in fibrotic GCs leads to a marked reduction in immune demarcation between malignant cells and fibroblasts in this GC subtype.

Malignant-dominant and malignant-infiltrated niches correspond to histologically defined tumour cores and invasive margins, respectively. It was postulated that malignant cells within these distinct histological areas exhibit unique gene expression profiles, a hypothesis that extends to other cell types, such as fibroblasts.[13 14] We thus investigated variations in expression among cells to shed light on the transcriptional behaviour of malignant and other cells in response to TME infiltration. Because the spot-level expression profiles encompass mixtures of various cell types, we used deconvolution techniques to infer cell type-specific expression data for five major cell types in the GC TME: malignant cells, normal epithelium, fibroblasts, endothelial cells and aggregated immune cells. Figure 2D presents a schematic that visualises the deconvolution process with reference to the different niches (online supplemental note 4). In this example, two cell types—malignant cells and fibroblasts—are shown in distinct spatial contexts: isolated regions (depicted on the left for malignant cells and on the right for fibroblasts) and areas of mutual infiltration (central region). The inferred expression profiles were largely segregated in accordance with their cell lineages, ensuring the accuracy of our cell type-specific expression profiling (figure 2E). Gene set enrichment analyses (GSEAs) on four of the major cell types (excluding normal epithelial cells) identified key molecular functions, which are shown in heatmaps in figure 2F (false discovery rate <0.1). Malignant cells in malignant-dominant niches showed gene upregulation associated with coagulation. In contrast, malignant cells in fibroblast-infiltrated niches exhibited increased expression of genes linked to the epithelial-to-mesenchymal transition (EMT), angiogenesis and allograft rejection functions were notably upregulated in malignant cells, fibroblasts, endothelial cells and immune cells within fibroblast-infiltrated niches, highlighting them as active zones in the GC TME. The expression levels of pathway genes for selected molecular functions (indicated by arrows in figure 2F) are shown across the niches (figure 2G, see online supplemental note 5 for the details). The GC subtype-based functional enrichment analyses are shown in online supplemental figure S5 to illustrate that the cell type-specific functional associations mentioned are particularly evident in epithelial and fibrotic GCs. The transcriptional levels of immune-related genes, including various immune exhaustion markers such as *IDO1, CTLA4, PDCD1* and *EOMES*, were also elevated in immune cells in fibroblast-infiltrated niches (figure 2H). The immune cell-specific expression profiles were further deconvoluted and shown for the immune-related genes across immune cell types (online supplemental figure S6), demonstrating that immune exhaustion markers such as *CTLA4* and *PDCD1* are transcriptionally upregulated in regulatory T cells (Tregs) among T cell populations. An abundance analysis of 22 immune cells revealed a higher prevalence of B cells and myeloid cells (dendritic cells and macrophages) in fibroblast-infiltrated niches, suggesting that fibroblast infiltration reconstitutes the immune cell composition in GC TMEs (figure 2I). The findings indicate that malignant cells in fibroblast-infiltrated niches are particularly aggressive. Additionally, immune cells, such as myeloid cells, located in those areas express exhaustion markers.

Landscape of intercellular crosstalk and its functional consequences

Although the niche analysis is informative about the effects of TME infiltration, it remains challenging to identify which cell types in the TME are specifically responsible for cellular interactions as regulators. Therefore, we devised a method for inferring both crosstalk between 'regulator' and 'target' cell types and its subsequent functional outcomes. Schematics for decoding those cellular interactions at the resolution of individual cell types are shown in figure 3A. See online supplemental note 6 and online supplemental figure S14 for the details. Major functional changes in the GC TME include the upregulation of genes associated with cellular proliferation, such as those for the G2M checkpoint, MYC targets and E2F targets (highlighted by a black box in figure 3B). That upregulation coincides with the infiltration of malignant and endothelial cells as regulator cells, suggesting that cells in the GC TME adapt to endothelial and malignant cell infiltration by enhancing cellular proliferation. To support that observation, we estimated the proliferation index using genes that represent cell proliferation. Then, we compared the cell type-specific proliferation index with the level of malignant cell infiltration (figure 3C) and endothelial cell infiltration (figure 3D) by categorising the spots into quintiles (with bin1 and bin5 representing the lowest and highest infiltration of malignant cell or endothelial cells, respectively). Notably, we found a consistent upward trend in the proliferation index that correlated with those infiltrations. This trend underlines the potential roles that malignant and endothelial cells play within

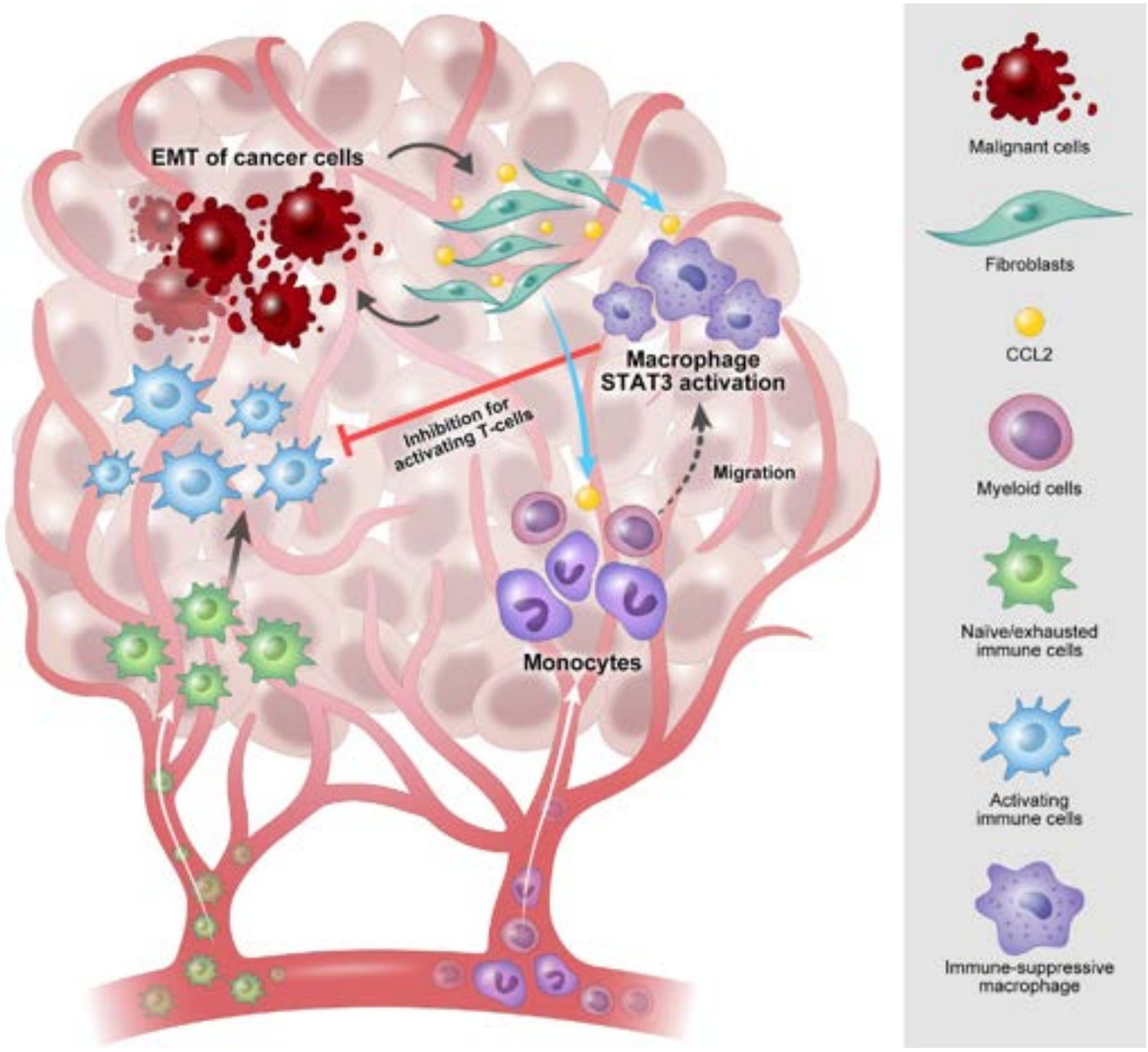

Figure 7 Cellular crosstalk mediated by cancer-associated fibroblasts (CAFs) leads to immunosuppressive tumour microenvironment (TME). The schematic depicts a gastric cancer (GC) TME in which CAFs facilitate the epithelial-to-mesenchymal transition (EMT) of malignant cells and recruit macrophages. The macrophages undergo in situ activation of STAT3, subsequently suppressing T cell activation and contributing to immune suppression in the GC TME.

the GC TME. We also observed that the upregulation of various immune-related functions (represented by eight hallmark gene sets) aligned with the infiltration of fibroblasts and immune cells as regulator cells. The eight immune-related gene sets were further segregated into those associated with the infiltration of immune cells (eg, responses to interferon (IFN)α and IFNγ, IL2-STAT5 signalling and allograft rejection) and those associated with fibroblasts' regulatory influence over malignant and immune cells (green and red boxes in figure 3B, respectively). The latter group includes pathways involved in inflammation-related immune responses such as tumour necrosis factor-α signalling through nuclear factor kappa B and IL6-JAK-STAT3 signalling, the inflammatory response and complement activation. Notably, within this immune-related cluster, the effects of endothelial cells on fibroblasts (depicted in the second column from the right in figure 3B) are observed, rather than cellular proliferation. We next focused on how fibroblast infiltration affects immune cells in terms of the eight identified immune-related functions (figure 3E). Across five bins of fibroblast infiltration levels (with bin1 and bin5 representing the lowest and highest fibroblast infiltration, respectively), we found a consistent increase in the scores of the eight immune-related gene sets, which were particularly pronounced in the functions of IL6-JAK-STAT3 and allograft rejection (figure 3E). We also examined the expression levels of individual immune-related genes among the bins of fibroblast infiltration (figure 3F). Whereas cytotoxic genes such as *GZMA* and *GZMB* were upregulated in spots with low fibroblast infiltration, immune checkpoints such as *PDCD1*, *CTLA4* and *TIGIT* tended to be upregulated as fibroblast infiltration increased, suggesting that these immune checkpoints are

upregulated during interactions with fibroblasts, which leads to immune cell dysfunctions in the GC TME. Those results imply that fibroblasts contribute to an immunosuppressive TME by activating the JAK-STAT3 signalling pathway in target cells.

CCL2+ cancer-associated fibroblasts regulate JAK-STAT3 signalling in macrophages

Among the functions of immune cells potentially modulated by fibroblasts (figure 3E), we focus on IL6-JAK-STAT3 because it is related to a procancerous, inflammatory response in GC TMEs.[15] We used a NicheNet analysis[16] to identify the key ligands in the regulator cells (fibroblasts) and their matching receptor and target genes in the receptor cells (immune cells). Figure 4A shows the ligands expressed in fibroblasts and the target and receptor genes expressed in immune cells. Among the ligands expressed in fibroblasts, *CCL2* emerged as a master regulator with extensive connections with target genes associated with IL6-JAK-STAT3 signalling (eg, *LTB, SOCS1, SOCS3, STAT3* and *TGFB1*). It also had the highest level of ligand activity in the NicheNet analysis. Additional regulators expressed by fibroblasts include known cancer-associated fibroblast (CAF) markers such as *TIMP-1* and *FN*.[17] The NicheNet analysis of the eight immune-related pathways (shown in figure 3B) further revealed that *CCL2* is consistently identified as a master regulator in seven out of the eight immune-related pathways (online supplemental figure S7). To further characterise the *CCL2* expression of fibroblasts in the GC TME, we used our previous scRNA-seq data for 726 fibroblasts obtained from five GC specimens.[9] In a t-Distributed Stochastic Neighbour Embedding plot representing the 726 fibroblasts, the expression level of *CCL2* is not widely distributed but rather localised in a cluster (figure 4B). We then explored the correlation between *CCL2* expression and other ligands, as well as the scores for inflammatory CAFs and myofibroblastic CAFs (figure 4C). Fibroblasts expressing *CCL2* (*CCL2+* fibroblasts) exhibit a distinct relationship with other fibroblast subtypes in GC TMEs (online supplemental note 7 and online supplemental figure S15). In all the single cells in the GC TME (n=23 477) of the reference,[9] a high JAK-STAT3 score was predominantly found in myeloid cells, particularly macrophages, indicating that macrophages are the primary immune cells expressing IL6-JAK-STAT3 activity (figure 4D). As a result, we categorised macrophages based on the activation of IL6-JAK-STAT3 signalling (the 251 *STAT3*-activated macrophages with high JAK-STAT3 scores vs the remaining 1804 macrophages). We also performed CellphoneDB cell-cell interaction analyses, which showed that among the top-scoring ligands (*CCL2*, *SAA1*, *CCL19* and *CCL21*), the number of interacting ligand-receptor gene pairs was higher in *CCL2+* fibroblasts and *STAT3*-activated macrophages compared with their *CCL2−* counterparts (figure 4E, online supplemental note 7 and online supplemental figure S16).

Subsequently, we identified gene markers for *CCL2+* fibroblasts and *STAT3*-activated macrophages using the CIBERSORT signature matrix functions, and we found 425 signature genes exclusive to each cell type (425 genes for *CCL2+* fibroblasts and 425 genes for *STAT3*-activated macrophages details provided in online supplemental table S3). We then examined whether the spatial presentation of *CCL2+* fibroblasts and *STAT3*-activated macrophages, based on their signature scores and their spatial correlation, indicates co-localisation. In GC1, a strong agreement was observed between the abundance of *CCL2+* fibroblasts and *STAT3*-activated macrophages based on their representative signature scores, indicating their co-localisation in GC TME (figure 4F). The correlation between the abundance of the major cell types and the signature scores of those two cell types was further examined across spots from the nine cases. That analysis confirmed a high degree of correlation between *CCL2+* fibroblasts and *STAT3*-activated macrophages, revealing that these two cell types predominantly cluster together with stromal cells, which also confirmed their co-localisation (figure 4G). The spatial co-localisation of these two cell types in other cases is illustrated in online supplemental figure S8. In addition, those results were validated using dual RNA *in situ* hybridisation (RNA-ISH) for *CCL2*/*COL1A1* genes and chromogen multiplex immunohistochemistry for pSTAT3/CD68 (online supplemental figure S9). Despite the overall concordance across cases, certain cases, such as GC9, exhibited a predominance of *CCL2+* fibroblasts, and others, such as GC4, showed a prevalence of *STAT3*-activated macrophages.

We further investigated the relationship between the signature scores of *CCL2+* fibroblasts and *STAT3*-activated macrophages and their association with clinical outcomes in GC. We obtained public bulk-level RNA-seq and microarray data with patient outcomes.[18–21] In the Asian Cancer Research Group (ACRG) and The Cancer Genome Atlas (TCGA) cohorts, we observed that most cases were either CF-high/SM-high or CF-low/SM-low: 84% (252 out of 300 cases) for ACRG and 87.6% (338 out of 386 cases) for TCGA, reflecting a strong correlation between the two signature scores. Thus, we focused on comparing those two groups (CF-high/SM-high vs CF-low/SM-low). That analysis revealed that patients in the CF-high/SM-high category exhibited significantly poorer prognosis than those in the other group in terms of overall survival (for ACRG and TCGA, p=0.02 and p=0.05, respectively, log-rank test, figure 4H). Details of the survival plots for the four categories and patient numbers are provided in online supplemental figure S10. Similar trends in clinical outcomes were observed in four other GC cohorts (GSE13861, GSE16899, GSE16901, GSE18541 with p=0.06, 0.04, 0.02, 0.09, respectively) (figure 4I). Those results suggest that *CCL2+* fibroblasts might promote GC progression and regulate an immunosuppressive TME via *STAT3*-activated macrophages.

CCL2+ CAFs recruit myeloid cells via *STAT3*-activated macrophages, leading to an immunosuppressive TME

To substantiate the findings from our spatial transcriptome analysis, we performed experiments in multiple *in vitro* models. Initially, we observed transcriptional upregulation of *CCL2* in various CAFs, compared with human immune and GC cell lines (online supplemental figure 11A). Subsequently, we demonstrated that conditioned medium (CM) from CAFs significantly increased the migration of a human monocyte cell line (THP-1) in a transwell migration assay (figure 5A). Treatment with neutralising *CCL2* antibody markedly decreased the migratory activity of CAF CM-stimulated THP-1 cells (figure 5B). We developed a *CCL2* knockdown CAF cell line using short hairpin RNA (online supplemental figure 11B) and found that the genetic inhibition of *CCL2* in CAFs reduced the CAF-induced migratory effect in THP-1 cells (figure 5C). Additionally, recombinant CCL2 protein also increased migration of THP-1 cells in a dose-dependent manner (online supplemental figure 11C,D). Next, we differentiated THP-1 cells into macrophages using phorbol 12-myristate 13-acetate (PMA) and co-cultured them with CAFs to evaluate transcription changes. GSEA revealed the upregulation of genes related to the JAK-STAT3 signalling pathway following CAF co-culture (figure 5D). A western blot

analysis confirmed the increased phosphorylation of STAT3 in macrophages co-cultured with various CAFs and also in macrophages treated with human recombinant CCL2 (figure 5E). Finally, we examined how CAF-stimulated macrophages affect human T cells. Jurkat T cells activated by PMA and ionomycin showed upregulation of the *INFG* gene, an immune-activated marker gene (figure 5F). Co-culture of these activated T cells with CAF-stimulated macrophages led to a significant reduction in *IFNG* gene expression (figure 5G). CAF-induced STAT3 activation in macrophage and the inhibition of T-cell activation by CAF-stimulated macrophages were successfully reproduced in experiments using macrophages and cytotoxic T-cells differentiated from human peripheral blood mononuclear cells (online supplemental figure 11E, F). These findings suggest that *CCL2*+ CAFs recruit myeloid cells to their vicinity in the GC TME and activate the STAT3 signalling pathway in macrophages, thereby serving as key regulators of the immunosuppressive TME in fibrotic GCs.

CCL2+ fibroblast-mixed syngeneic mouse tumours recapitulate histological characteristics of fibrotic GC with immunosuppressive TME

We established syngeneic tumours using the YTN3 mouse GC cell line with and without a mouse gastric fibroblast (MGF) cell line stably expressing GFP (green fluorescent protein) (online supplemental figure 12A). First, we screened *CCL2* expression across various mouse cell lines (GFP+MGF, mouse GC and immune cells). The highest *CCL2* expression was observed in the GFP+MGFs (online supplemental figure 12B). After injecting tumour cells into mice, we harvested the tumours 7, 14 and 26 days later (figure 6A). We observed that YTN3 tumours mixed with GFP+MGF cells were larger than tumours containing only YTN3 cells at 14 days postinjection (figure 6B and online supplemental figure 12C). Immunohistochemical staining for GFP and smooth muscle actin affirmed the sustained presence of mixed GFP+MGF cells within the tumours. The tumours with mixed MGF cells exhibited characteristics reminiscent of fibrotic subtype GCs (figure 6C). We also stained the harvested tumours with mouse immune cell markers for macrophages (F4/80), cytotoxic T cells (CD8α) and the immune activating marker granzyme B (Grz B). The results showed an enrichment of macrophages in MGF-mixed tumours, accompanied by a reduced accumulation of CD8+ T cells and Grz B+ cells in the central region of tumours, compared with YTN3-only tumours (figure 6D). These animal experiments demonstrated that *CCL2*+ fibroblasts enhanced macrophage accumulation in syngeneic tumours and contributed to an immunosuppressive TME.

Validation of GC subclassification and co-localisation of two cell types (*CCL2*+ fibroblasts and pSTAT3-activated macrophages) in a large GC cohort

For histological validation, we obtained tissue microarrays (TMAs) of 675 GC cases. We calculated the ratio of the DAB (3,3′-diaminobenzidine) staining area in the entire TMA core. Based on the three cellular abundance-based GC subtypes we identified (figure 1), we classified the 675 GC cases into 228 epithelial, 126 immunogenic and 321 fibrotic GCs according to whether immunohistochemistry (IHC) showed that pancytokeratin, CD45RB and actin protein, respectively, had the highest expression (figure 6E). We found a significantly large number of differentiated-type GCs in the epithelial subgroup, whereas the immunogenic subgroup accounted for a large portion of undifferentiated-type GCs ($p<0.001$).[22] In addition, we found significantly more MSI-H GCs in the epithelial subtype and more EBV-positive GCs in the immunogenic subtype ($p<0.001$ and $p=0.004$, respectively). The clinicopathological characteristics of the enrolled patients according to the three GC subtypes are shown in online supplemental table S4. Next, we performed a survival analysis and found obvious differences in overall survival between fibrotic and non-fibrotic subgroups. As shown in figure 6E (right panel), the fibrotic subtype showed worse prognosis than non-fibrotic subtypes (log-rank test, $p=0.015$). Those findings further confirmed that fewer immune cells infiltrate into fibrotic GCs than into the other types, leading to worse clinical outcomes in an independent cohort. Additionally, we confirmed co-localisation of *CCL2*+ fibroblasts and pSTAT3+ macrophages in a subset of TMA tissues using RNA-ISH and multiplex IHC (online supplemental note 8 and online supplemental figure S17). These findings support the spatial co-localisation of these two cell types in the spatial transcriptomics using Visium technologies and highlight its clinical meaning.

DISCUSSION

In this study, Visium technology[11] for spatial transcriptomics was used to analyse the TMEs of nine GC specimens. To address that the limited spatial resolution, deconvolution techniques are crucial for analysing Visium-based spatial transcriptomics data.[23 24] Based on deconvolution, we initially identified three primary GC subtypes: immunogenic, epithelial and fibrotic GCs. Immunogenic GCs such as GC1 are characterised by a diverse immune cell population that includes T cells and PCs, similar to the immune-inflamed[25] or immune-hot tumours.[26] On the other hand, epithelial GCs display a marked reduction in T cells and PCs, but consistently maintain myeloid cells and B cells. Fibrotic GCs, meanwhile, demonstrate extensive infiltration of fibroblasts alongside a notable decrease in T cells and PCs. As previously proposed,[27 28] the depletion of both CD4+ and CD8+ T cells in fibrotic GCs could be mediated by interactions between fibroblasts and other types of immune or TME cells.

To delineate the spatial architecture of the GC TME, we developed two methodologies: one based on spot-clusters as recurring units of tissue subarchitecture (niches) and the other based on the inference of spot-level, cell type-specific expression. We used niches to classify the tissue architecture into six categories based on the cellular composition and to cluster spots to infer cell type-specific expression, thereby delineating the transcriptional dynamics of individual cell types with respect to their immediate cellular contexts. Some of earlier deconvolution methods also aimed to identify the expression profiles of individual cell types, a process known as reference-free deconvolution.[29 30] In spatial transcriptomics, determining cell type-specific expression in cancer tissues is more complicated than in non-cancerous tissues. As one solution, we opted to restrict the number of cell types to be deconvoluted (eg, focusing on the five major cell types, as previously recommended).[31] Moreover, we used the niches as TME-aware spot groups to determine cell type-specific gene expression.[31] As a result, tissue architecture-aware approaches based on spatial transcriptome data provide evidence about the actual effects of TME infiltration on individual cell types. Although the EMT is heightened in fibroblasts within fibroblast-enriched niches, the EMT-related genes in fibroblasts (mainly CAF activation markers) differ from those in malignant cells (mainly transforming growth factor (TGF) β signalling genes) suggesting that a fibroblast-enriched TME could facilitate the activation of CAF-mediated TGFβ signalling in malignant cells and CAF activation in fibroblasts.[32] Of

note, the cancer hallmarks, for example, EMT in malignant cells, angiogenesis in endothelial cells and allograft rejection in immune cells, are pronounced in fibroblast-infiltrated niches. Additionally, the deconvolution of immune marker gene expression across immune cell types suggests that exhaustion markers, such as *CTLA4*, are transcriptionally upregulated in Tregs. However, due to technical limitations of the deconvolution process, the transcriptional dynamics of T cell subpopulations, such as cytotoxic T cells, were not evaluated. Further investigation using high-resolution spatial platforms will be required to evaluate these subpopulations.

The cellular composition across niche types revealed that while niches dominated by specific cell types largely depend on the GC subtypes, niches characterised by cellular interactions, such as malignant-infiltrated and fibroblast-infiltrated niches, remain relatively consistent across GC subtypes. This suggests that malignant cells and fibroblasts occupy significant spatial niches where they actively engage in cell-cell interactions. To further examine the cell-cell interactions in spatial scale, we next built a landscape of cellular crosstalk among individual cell types. This map proposed several hypotheses about functional relationships between regulator and target cell types. One observation is that endothelial and malignant cells that infiltrate the TME might promote tumour growth by upregulating genes linked to cell proliferation. That finding is consistent with previous observations of TME responses to proliferating malignant cells.[33] It is also possible that increased endothelial cell infiltration leads to defective angiogenesis, and the resulting hypoxic conditions could be associated with overall cellular proliferation in the TME.[34] Among the hypotheses about the effects of fibroblasts, we focused on how they affect IL6-JAK-STAT3 and inflammatory signalling in immune cells. Of note, JAK-STAT3 signalling is restricted to macrophages, which further refines the hypothesis that *CCL2*+ fibroblasts trigger a procancer inflammatory response in macrophages in the GC TME. We further assert that *CCL2*+ fibroblasts and *STAT3*-activated macrophages could be key interacting cell subtypes in the GC TME. Their co-localisation in spatial data and their clinical association, that is, co-infiltration of *CCL2*+ fibroblasts and *STAT3*-activated macrophages associated with unfavourable clinical outcomes, could make them potential cell-based targets for therapeutic interventions and personalised treatment strategies.

CCL2, which is an important molecule in the attraction and activation of macrophages across various diseases,[35–37] plays a multifaceted role in malignant tumours. It has been implicated in recruiting immunosuppressive myeloid cells, including myeloid-derived suppressor cells,[38 39] In our recent study, we demonstrated that *CCL2*+ fibroblasts play a pivotal role in regulating the immune microenvironment within GC tissues.[9] Notably, the monoclonal antibody for *CCL2*, known as carlumab or CNTO888, did not exhibit significant efficacy as monotherapy in end-stage solid tumours.[40] However, our present study suggests that *CCL2*-targeting therapy might yield synergistic effects if combined with immune checkpoint inhibitors (ICIs), particularly in fibrotic subtypes of GC. The efficacy of targeting *CCL2* or the cognate receptor *CCR2*, for this GC type should be evaluated in the future to facilitate the application of that strategy in clinical settings.

ICIs have emerged as third-generation anticancer drugs; however, the results from three representative clinical trials have shown heterogeneity, with minimal improvement in survival.[41–43] The potential markers, such as programmed cell death protein 1 expression, MSI or positive EBV status, might predict a positive response to ICIs. However, they do not fully account for the role of the TME in ICI resistance.[44] Transcriptome analyses using bulk GC tissues revealed that fibroblast-enriched subclusters presented an immunosuppressive TME and were expected to exhibit a poor response to ICIs.[45] Our results suggest that *CCL2*+ fibroblasts play a key role in regulating this mechanism, making them a potential target for shifting immune-cold tumours into an immune-hot state, particularly in the fibrotic GC subtype. Such a shift could enhance the response to ICIs and ultimately improve treatment outcomes (figure 7).

In conclusion, the findings from this study provide valuable insight into the spatial and cellular heterogeneity of GCs, illuminating the intricate interactions among different cell types within GC TMEs. These findings hold promise for informing the development of novel therapeutics and advancing understanding of the cellular mechanisms involved in GC progression and prognosis. Nonetheless, additional research and clinical validation are needed to translate these findings into actionable strategies that could benefit patients with GC.

Author affiliations
[1]Department of Hospital Pathology, Seoul St. Mary's Hostpital, Collage of Medicine, The Catholic University of Korea, Seoul, The Republic of Korea
[2]Department of Surgery, Ajou University School of Medicine, Suwon, The Republic of Korea
[3]Cancer Biology Graduate Program, Ajou University School of Medicine, Suwon, The Republic of Korea
[4]Inflamm-Aging Translational Research Center, Ajou University School of Medicine, Suwon, The Republic of Korea
[5]Department of Medical Informatics, College of Medicine, The Catholic University of Korea, Seoul, The Republic of Korea
[6]Department of Biomedicine & Health Sciences, Graduate School, The Catholic University of Korea, Seoul, The Republic of Korea
[7]Department of Pathology, Asan Medical Center, University of Ulsan, College of Medicine, Seoul, The Republic of Korea
[8]Division of Gastrointestinal Surgery, Department of Surgery, Seoul St. Mary's Hospital, College of Medicine, The Catholic University of Korea, Seoul, The Republic of Korea
[9]Department of Surgery, Yonsei University, Seoul, The Republic of Korea
[10]Cancer Research Institute, College of Medicine, The Catholic University of Korea, Seoul, The Republic of Korea
[11]CMC Institute for Basic Medical Science, the Catholic Medical Center of The Catholic University of Korea, Seoul, The Republic of Korea

Acknowledgements We appreciate the support for this research from the Basic Medical Science Facilitation Programme through the Catholic Medical Center of the Catholic University of Korea, funded by the Catholic Education Foundation. The biospecimens and data used in this study were provided by the Ajou Human Bio-Resource Bank (AHBB), a member of the National Biobank of Korea, which is supported by the Ministry of Health and Welfare.

Contributors SHL, DL, HH and T-MK designed the study. JC developed the methodology. SHL, DL and JC acquired data. SHL and DL analysed and interpreted data. SHL, DL, HH and T-MK wrote and reviewed the manuscript. HJO, I-HH, DR, S-YL, D-JH, SK, YM, IHS, KYS, HL and SL provided technical and material support. HH and T-MK are the guarantors of this work and fully responsible for the overall work and the conduct of the study.

Funding This study was supported by the National Research Foundation of Korea (NRF) (2019M3E5D3073104 and 2019R1A5A2027588 to T-MK, 2022R1A2C2010644 to SHL), the Ministry of Education of Korea (2020R1A6A1A03043539 to HH) and the Bio&Medical Technology Development Programme of NRF funded by the Korean government (MSIT) (RS-2023-00221174 to HH).

Competing interests None declared.

Patient and public involvement Patients and/or the public were not involved in the design, or conduct, or reporting, or dissemination plans of this research.

Patient consent for publication Not applicable.

Ethics approval This study was approved by the AJOU University Institutional Review Board (AJOUIRB), AJOUIRB-EXP-2022-099 and AJOUIRB-EX-2024-356, and the Institutional Review Board of The Catholic University of Korea, Seoul St. Mary's Hospital (KC22SASI0245). Participants provided informed consent before taking part in the study.

Provenance and peer review Not commissioned; externally peer reviewed.

Data availability statement Data are available in a public, open access repository. The datasets analysed in the current study are available in the TCGA Research Network (https://www.cancer.gov/tcga) and Gene Expression Omnibus (GEO) with accession ID GSE62254, GSE13861, GSE268999, GSE26901 and GSE28541. The sequencing data have been uploaded to GEO with accession ID GSE251950.

ORCID iD

Dagyeong Lee http://orcid.org/0000-0002-6542-6526

REFERENCES

1 Yeoh KG, Tan P. Mapping the genomic diaspora of gastric cancer. *Nat Rev Cancer* 2022;22:71–84.
2 Nakamura Y, Kawazoe A, Lordick F, *et al*. Biomarker-targeted therapies for advanced-stage gastric and gastro-oesophageal junction cancers: an emerging paradigm. *Nat Rev Clin Oncol* 2021;18:473–87.
3 Bang Y-J, Van Cutsem E, Feyereislova A, *et al*. Trastuzumab in combination with chemotherapy versus chemotherapy alone for treatment of HER2-positive advanced gastric or gastro-oesophageal junction cancer (ToGA): a phase 3, open-label, randomised controlled trial. *Lancet* 2010;376:687–97.
4 Kim T-H, Kim I-H, Kang SJ, *et al*. Korean Practice Guidelines for Gastric Cancer 2022: An Evidence-based, Multidisciplinary Approach. *J Gastric Cancer* 2023;23:3–106.
5 Zhang P, Yang M, Zhang Y, *et al*. Dissecting the Single-Cell Transcriptome Network Underlying Gastric Premalignant Lesions and Early Gastric Cancer. *Cell Rep* 2019;27:1934–47.
6 Sathe A, Grimes SM, Lau BT, *et al*. Single-Cell Genomic Characterization Reveals the Cellular Reprogramming of the Gastric Tumor Microenvironment. *Clin Cancer Res* 2020;26:2640–53.
7 Zhang M, Hu S, Min M, *et al*. Dissecting transcriptional heterogeneity in primary gastric adenocarcinoma by single cell RNA sequencing. *Gut* 2021;70:464–75.
8 Kumar V, Ramnarayanan K, Sundar R, *et al*. Single-Cell Atlas of Lineage States, Tumor Microenvironment, and Subtype-Specific Expression Programs in Gastric Cancer. *Cancer Discov* 2022;12:670–91.
9 Jeong HY, Ham I-H, Lee SH, *et al*. Spatially Distinct Reprogramming of the Tumor Microenvironment Based On Tumor Invasion in Diffuse-Type Gastric Cancers. *Clin Cancer Res* 2021;27:6529–42.
10 Asp M, Bergenstråhle J, Lundeberg J. Spatially Resolved Transcriptomes-Next Generation Tools for Tissue Exploration. *Bioessays* 2020;42:e1900221.
11 Ståhl PL, Salmén F, Vickovic S, *et al*. Visualization and analysis of gene expression in tissue sections by spatial transcriptomics. *Science* 2016;353:78–82.
12 Cho J, Chang YH, Heo YJ, *et al*. Four distinct immune microenvironment subtypes in gastric adenocarcinoma with special reference to microsatellite instability. *ESMO Open* 2018;3:e000326.
13 Arora R, Cao C, Kumar M, *et al*. Spatial transcriptomics reveals distinct and conserved tumor core and edge architectures that predict survival and targeted therapy response. *Nat Commun* 2023;14:5029.
14 Xun Z, Ding X, Zhang Y, *et al*. Reconstruction of the tumor spatial microenvironment along the malignant-boundary-nonmalignant axis. *Nat Commun* 2023;14:933.
15 Owen KL, Brockwell NK, Parker BS. JAK-STAT Signaling: A Double-Edged Sword of Immune Regulation and Cancer Progression. *Cancers (Basel)* 2019;11:2002.
16 Browaeys R, Saelens W, Saeys Y. NicheNet: modeling intercellular communication by linking ligands to target genes. *Nat Methods* 2020;17:159–62.
17 Zhang H, Yue X, Chen Z, *et al*. Define cancer-associated fibroblasts (CAFs) in the tumor microenvironment: new opportunities in cancer immunotherapy and advances in clinical trials. *Mol Cancer* 2023;22:159.
18 The Cancer Genome Atlas Research Network. Comprehensive molecular characterization of gastric adenocarcinoma. *Nature New Biol* 2014;513:202–9.
19 Cristescu R, Lee J, Nebozhyn M, *et al*. Molecular analysis of gastric cancer identifies subtypes associated with distinct clinical outcomes. *Nat Med* 2015;21:449–56.
20 Cho JY, Lim JY, Cheong JH, *et al*. Gene expression signature-based prognostic risk score in gastric cancer. *Clin Cancer Res* 2011;17:1850–7.
21 Oh SC, Sohn BH, Cheong J-H, *et al*. Clinical and genomic landscape of gastric cancer with a mesenchymal phenotype. *Nat Commun* 2018;9:1777.
22 Japanese Gastric Cancer Association. Japanese Gastric Cancer Treatment Guidelines 2021 (6th edition). *Gastric Cancer* 2023;26:1–25.
23 Li B, Zhang W, Guo C, *et al*. Benchmarking spatial and single-cell transcriptomics integration methods for transcript distribution prediction and cell type deconvolution. *Nat Methods* 2022;19:662–70.
24 Li H, Zhou J, Li Z, *et al*. A comprehensive benchmarking with practical guidelines for cellular deconvolution of spatial transcriptomics. *Nat Commun* 2023;14:1548.
25 Chen Y, Sun Z, Chen W, *et al*. The Immune Subtypes and Landscape of Gastric Cancer and to Predict Based on the Whole-Slide Images Using Deep Learning. *Front Immunol* 2021;12:685992.
26 Bagaev A, Kotlov N, Nomie K, *et al*. Conserved pan-cancer microenvironment subtypes predict response to immunotherapy. *Cancer Cell* 2021;39:845–65.
27 Costa A, Kieffer Y, Scholer-Dahirel A, *et al*. Fibroblast Heterogeneity and Immunosuppressive Environment in Human Breast Cancer. *Cancer Cell* 2018;33:463–79.
28 Ene-Obong A, Clear AJ, Watt J, *et al*. Activated pancreatic stellate cells sequester CD8+ T cells to reduce their infiltration of the juxtatumoral compartment of pancreatic ductal adenocarcinoma. *Gastroenterology* 2013;145:1121–32.
29 Ma Y, Zhou X. Spatially informed cell-type deconvolution for spatial transcriptomics. *Nat Biotechnol* 2022;40:1349–59.
30 Miller BF, Huang F, Atta L, *et al*. Reference-free cell type deconvolution of multi-cellular pixel-resolution spatially resolved transcriptomics data. *Nat Commun* 2022;13:2339.
31 Newman AM, Steen CB, Liu CL, *et al*. Determining cell type abundance and expression from bulk tissues with digital cytometry. *Nat Biotechnol* 2019;37:773–82.
32 Yu Y, Xiao C-H, Tan L-D, *et al*. Cancer-associated fibroblasts induce epithelial-mesenchymal transition of breast cancer cells through paracrine TGF-β signalling. *Br J Cancer* 2014;110:724–32.
33 Anderson NM, Simon MC. The tumor microenvironment. *Curr Biol* 2020;30:R921–5.
34 Feitelson MA, Arzumanyan A, Kulathinal RJ, *et al*. Sustained proliferation in cancer: Mechanisms and novel therapeutic targets. *Semin Cancer Biol* 2015;35 Suppl:S25–54.
35 Aiello RJ, Bourassa PA, Lindsey S, *et al*. Monocyte chemoattractant protein-1 accelerates atherosclerosis in apolipoprotein E-deficient mice. *Arterioscler Thromb Vasc Biol* 1999;19:1518–25.
36 Antonelli A, Fallahi P, Delle Sedie A, *et al*. High values of Th1 (CXCL10) and Th2 (CCL2) chemokines in patients with psoriatic arthritis. *Clin Exp Rheumatol* 2009;27:22–7.
37 Jiang S, Wang Q, Wang Y, *et al*. Blockade of CCL2/CCR2 signaling pathway prevents inflammatory monocyte recruitment and attenuates OVA-Induced allergic asthma in mice. *Immunol Lett* 2019;214:30–6.
38 Huang B, Lei Z, Zhao J, *et al*. CCL2/CCR2 pathway mediates recruitment of myeloid suppressor cells to cancers. *Cancer Lett* 2007;252:86–92.
39 Qian B-Z, Li J, Zhang H, *et al*. CCL2 recruits inflammatory monocytes to facilitate breast-tumour metastasis. *Nature New Biol* 2011;475:222–5.
40 Pienta KJ, Machiels J-P, Schrijvers D, *et al*. Phase 2 study of carlumab (CNTO 888), a human monoclonal antibody against CC-chemokine ligand 2 (CCL2), in metastatic castration-resistant prostate cancer. *Invest New Drugs* 2013;31:760–8.
41 Janjigian YY, Shitara K, Moehler M, *et al*. First-line nivolumab plus chemotherapy versus chemotherapy alone for advanced gastric, gastro-oesophageal junction, and oesophageal adenocarcinoma (CheckMate 649): a randomised, open-label, phase 3 trial. *Lancet* 2021;398:27–40.
42 Kang Y-K, Chen L-T, Ryu M-H, *et al*. Nivolumab plus chemotherapy versus placebo plus chemotherapy in patients with HER2-negative, untreated, unresectable advanced or recurrent gastric or gastro-oesophageal junction cancer (ATTRACTION-4): a randomised, multicentre, double-blind, placebo-controlled, phase 3 trial. *Lancet Oncol* 2022;23:234–47.
43 Shitara K, Van Cutsem E, Bang Y-J, *et al*. Efficacy and Safety of Pembrolizumab or Pembrolizumab Plus Chemotherapy vs Chemotherapy Alone for Patients With First-line, Advanced Gastric Cancer: The KEYNOTE-062 Phase 3 Randomized Clinical Trial. *JAMA Oncol* 2020;6:1571–80.
44 Petitprez F, Meylan M, de Reyniès A, *et al*. The Tumor Microenvironment in the Response to Immune Checkpoint Blockade Therapies. *Front Immunol* 2020;11:784.
45 Zeng D, Li M, Zhou R, *et al*. Tumor Microenvironment Characterization in Gastric Cancer Identifies Prognostic and Immunotherapeutically Relevant Gene Signatures. *Cancer Immunol Res* 2019;7:737–50.